ARTICLES
https://doi.org/10.1038/s41561-018-0284-4
nature geoscience

Antarctic ice-sheet sensitivity to obliquity forcing enhanced through ocean connections

R. H. Levy[1,2*], S. R. Meyers[3], T. R. Naish[2], N. R. Golledge[1,2], R. M. McKay[2], J. S. Crampton[1,4], R. M. DeConto[5], L. De Santis[6], F. Florindo[7], E. G. W. Gasson[8], D. M. Harwood[9], B. P. Luyendyk[10], R. D. Powell[11], C. Clowes[1] and D. K. Kulhanek[12]

Deep sea geological records indicate that Antarctic ice-sheet growth and decay is strongly influenced by the Earth's astronomical variations (known as Milankovitch cycles), and that the frequency of the glacial–interglacial cycles changes through time. Here we examine the emergence of a strong obliquity (axial tilt) control on Antarctic ice-sheet evolution during the Miocene by correlating the Antarctic margin geological records from 34 to 5 million years ago with a measure of obliquity sensitivity that compares the variance in deep sea sediment core oxygen-isotope data at obliquity timescales with variance of the calculated obliquity forcing. Our analysis reveals distinct phases of ice-sheet evolution and suggests the sensitivity to obliquity forcing increases when ice-sheet margins extend into marine environments. We propose that this occurs because obliquity-driven changes in the meridional temperature gradient affect the position and strength of the circum-Antarctic easterly flow and enhance (or reduce) ocean heat transport across the Antarctic continental margin. The influence of obliquity-driven changes in ocean dynamics is amplified when marine ice sheets are extensive, and sea ice is limited. Our reconstruction of the Antarctic ice-sheet history suggests that if sea-ice cover decreases in the coming decades, ocean-driven melting at the ice-sheet margin will be amplified.

Insight into the causes of Antarctic ice sheet (AIS) variability—over a range of timescales—is fundamental to our understanding of the Earth-system response to climate change. Large-scale shifts in AIS volume and extent are controlled by changes in atmospheric carbon dioxide (CO_2) (refs. [1,2]) and plate tectonic processes[3] and usually occur over extended periods of time (hundreds of thousands to several million years). Geological snap-shots from the Antarctic margin show that higher-frequency oscillations in the AIS (glacial–interglacial episodes) were paced by astronomical variations in insolation that involve eccentricity[4,5] (orbital shape, ~400 and 100 kyr), obliquity[6] (axial tilt, 41 kyr) and precession[4] (wobble of the Earth's axis, ~20 kyr) cycles. Near-continuous records of ice-volume variation captured in oxygen isotope records ($\delta^{18}O$) from deep ocean sediment cores[7–10] show that the frequency of glacial–interglacial variability has evolved over the past 34 Myr (Fig. 1a). For example, glacial cycles during the Oligocene through the early Miocene were primarily paced by changes in long- and short-period eccentricity[8,9], whereas the influence of obliquity increased during the mid-Miocene climate transition (MCT)[10] and became dominant during portions of the late Miocene. These observations of variable ice-sheet response from both direct records at ice proximal locations and indirect geochemical proxies present a conundrum. It is well-established that changes in the Earth's astronomical configuration affect insolation in a predictable manner[11] so why was the AIS more sensitive to specific astronomical frequencies at different times? Ultimately, this feature suggests key transitions in the behaviour of the AIS related to ice-sheet size and dynamics (for example, terrestrial- versus marine-based ice sheets).

To address this question, we conducted a novel assessment of ice volume and high latitude surface temperature sensitivity to obliquity forcing (Fig. 1), computed from the deep marine $\delta^{18}O$ proxy record[7], and integrated this assessment with AIS-proximal geological records from the Antarctic continental shelf and a sea-level record from the New Jersey continental margin[12]. We acknowledge that high-resolution age control on geological sequences from the Earth's continental margins is often hard to achieve, but submit that correlations between records at the $>10^5$ kyr resolution required for this study are robust. These geographically distributed data sets are considered with modern observations and modelling studies to examine the evolving influence of astronomical forcing on Antarctica. As will be demonstrated through this synthesis, obliquity sensitivity (S_{obl}) provides a palaeosensor for the detection of terrestrial versus marine-based ice sheets, and thus sheds new light on the evolution of the AIS. To focus exclusively on the AIS, we restricted our analysis on the period from 34 to 5 million years ago (Ma), as the past five million years of Earth's history is characterized by the increasing influence of ice sheets in the Northern Hemisphere.

S_{obl} in the Earth system

We calculated S_{obl} by dividing obliquity variance in a $\delta^{18}O$ megasplice[7] by the variance of the theoretical obliquity solution[11] (Methods). Three distinct episodes in S_{obl} are revealed. A relatively low S_{obl} punctuated by small increases every 2.4 Myr characterizes the Oligocene. A substantial increase in S_{obl} occurs in the latest Oligocene, and the early-to-mid-Miocene is characterized by a

[1]GNS Science, Lower Hutt, New Zealand. [2]Antarctic Research Centre, Victoria University of Wellington, Wellington, New Zealand. [3]Department of Geoscience, University of Wisconsin—Madison, Madison, WI, USA. [4]School of Geography, Environment and Earth Science, Victoria University of Wellington, Wellington, New Zealand. [5]Department of Geosciences, University of Massachusetts, Amherst, MA, USA. [6]Istituto Nazionale di Oceanografia e di Geofisica Sperimentale (OGS), Sgonico, Trieste, Italy. [7]Istituto Nazionale di Geofisica e Vulcanologia (INGV), Roma, Italy. [8]School of Geographical Sciences, University of Bristol, Bristol, UK. [9]Earth & Atmospheric Sciences, University of Nebraska, Lincoln, Lincoln, NE, USA. [10]Earth Science Department, University of California, Santa Barbara, Santa Barbara, CA, USA. [11]Department of Geology and Environmental Geosciences, Northern Illinois University, DeKalb, IL, USA. [12]International Ocean Discovery Program, Texas A&M University, College Station, TX, USA. *e-mail: r.levy@gns.cri.nz

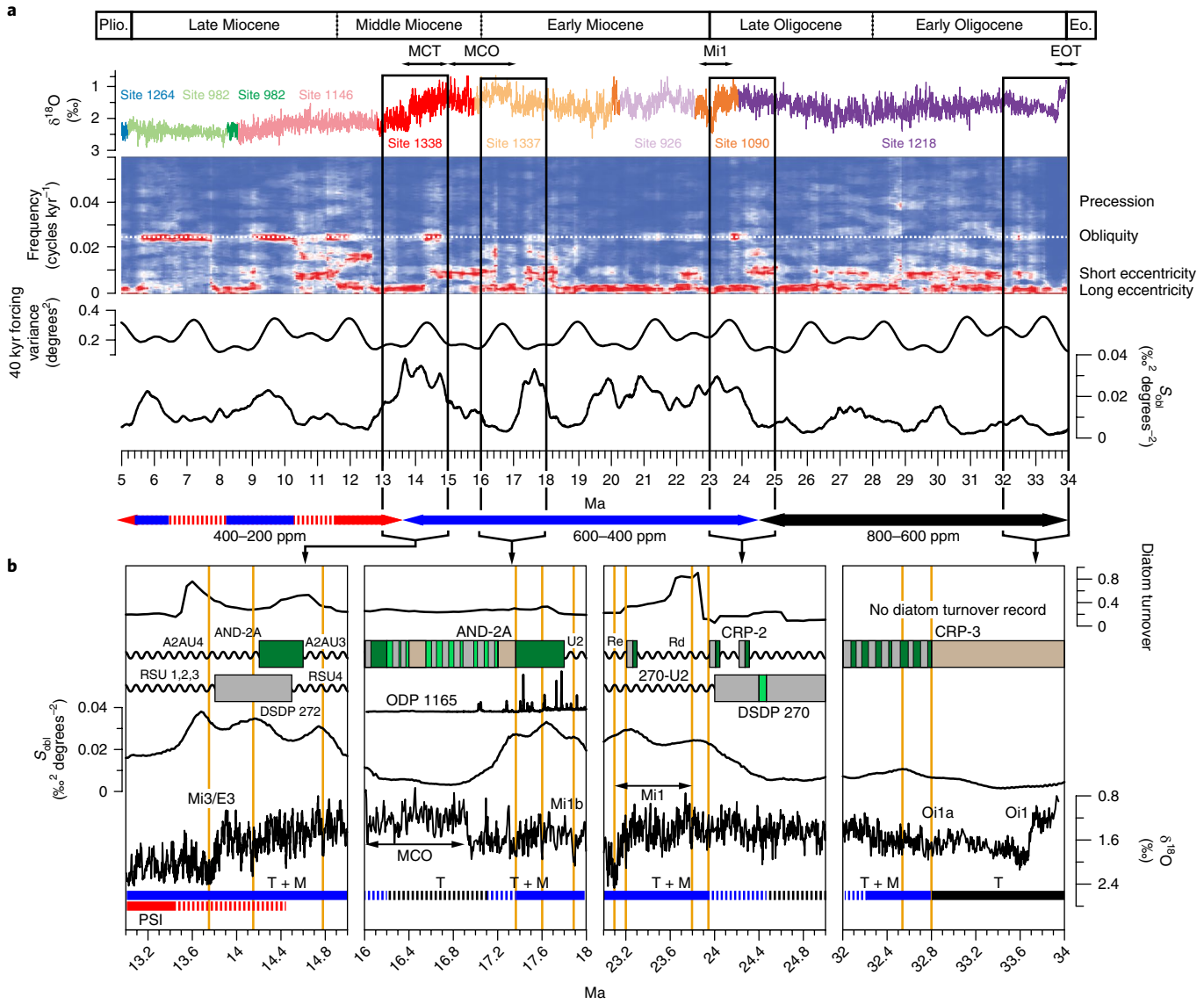

Fig. 1 | Integrated oxygen isotope data and Antarctic geological records. a, Oxygen isotope ($\delta^{18}O$) megasplice compilation[7] and evolutive power spectra (normalized such that the maximum power in each 1 Myr window is unity; deep red indicates maximum power, deep blue indicates minimum power). S_{obl} calculated from the obliquity forcing variance and the $\delta^{18}O$ record. Horizontal arrows show phases of AIS evolution reflected by major changes in S_{obl} (black, terrestrial; blue, episodic marine; red, perennial sea ice). Numbers in ppm indicate average range of atmospheric carbon dioxide concentration. **b**, Selected time intervals showing the correlation between S_{obl}, Antarctic geological records and $\delta^{18}O$ data. Colours in the drill core columns represent generalized stratigraphy (sinusoidal line, disconformity; dark green, grounding zone proximal diamictite; light green, distal glacial–marine diamictite; brown, sandstone with ice rafted debris; grey, mudstone). Vertical orange lines indicate episodes of maximum marine ice-sheet advance. Coloured bars reflect the ice-sheet extent: T, terrestrial (black); T + M, terrestrial and marine (blue), PSI, perennial sea ice (red); dashed lines, transitional. Eo., Eocene; Plio., Pliocene; EOT, Eocene–Oligocene transition; MCO, Miocene Climate Optimum; MCT, Miocene climate transition; Oi1, Oi1a, Mi1, Mi1b, Mi3 and E3, major oxygen isotope events; RSU, Ross Sea unconformity; Rd, Re, regional unconformities in Cape Roberts Project drillcores; A2AU2, U3 and U4, unconformities in ANDRILL-2A drillcore.

high S_{obl} variation. The maximum S_{obl} was reached during the MCT between ~14.8 and 13.8 Ma. After the MCT, S_{obl} decreased to low baseline values comparable to those of the Oligocene, but included episodes of moderate S_{obl}. We compared computed S_{obl} with the direct evidence of AIS variability from the Antarctic continental shelf (Figs. 1 and 2), to examine the influence of ice sheets on S_{obl}. We focus on the Ross Sea (Fig. 2) because well-dated drill cores and seismic profiles across the region provide a composite stratigraphy from the Eocene to Pleistocene linked to glacial processes that help constrain the glacial history[5,6,13–17]. Unfortunately, stratigraphic records from other regions of Antarctica's continental shelf are few and are difficult to date precisely due to the discontinuous core recovery[18–20]. However, numerical models indicate that ice-sheet variability in the Ross Sea reflects large-scale changes across the continent (Supplementary Fig. 1) and suggest that major environmental shifts captured in the geological records from the Ross Sea occurred in other regions of Antarctica at the same time.

Three phases of AIS evolution

Large continental-scale ice sheets became established on the Antarctic continent across the Eocene–Oligocene transition[5,21]. However, expansion into marine settings at the margins of the

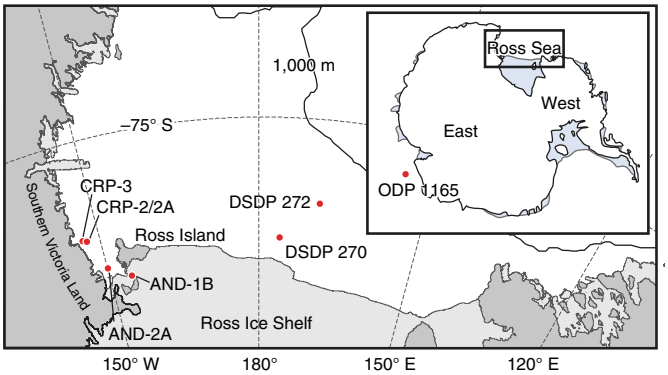

Fig. 2 | Antarctic location map with Ross Sea detail. Drill cores discussed here include CRP-2/2A and -3, AND-2A and -1B, DSDP sites 270 and 272, and ODP Site 1165. The 1,000 m bathymetric contour marks the approximate position of the modern continental shelf margin.

Ross Sea did not occur until 32.8 Ma, evidenced by an increase in glacimarine sediments in the Cape Roberts Project (CRP)-3 drill core[5]. This increase coincides with a small peak in S_{obl} (Fig. 1). Subsequent maxima in S_{obl} through the Oligocene occur every 2.4 Myr and coincide with disconformities in Ross Sea drill cores (Fig. 1 and Supplementary Table 1), which reflect the advance of ice beyond the Southern Victoria Land coastal margin. These data suggest that increases in S_{obl} occurred when outlet glaciers advanced beyond their terrestrial margins into marine environments and that the Earth system became more sensitive to obliquity forcing when small regions of the AIS were connected to the ocean. However, most of the Oligocene is characterized by low S_{obl}, and 100 and 400 kyr cycles dominate the $\delta^{18}O$ records[9] (Fig. 1), which suggests that Antarctica's terrestrial ice sheets were most sensitive to changes in atmospheric temperatures paced by variations in eccentricity and precession, consistent with direct insolation forcing.

A prominent increase in S_{obl} between 24.5 and 24 Ma marks one of the most significant environmental transitions in Antarctica since the Eocene–Oligocene transition (Fig. 1). The first occurrence of ice proximal glacimarine sediments in the Deep Sea Drilling Project (DSDP) Site 270[22], disconformities in CRP-2/2A[23], a large turnover in Southern Ocean phytoplankton (Fig. 1, Methods and Supplementary Fig. 2) and the seismic data[14] suggest that the first major expansion of marine ice sheets across the Ross Sea continental shelf occurred during this time interval. Proxy data indicate that CO_2 concentrations dropped below 600 ppm in the latest Oligocene and remained below this value through most of the Neogene[2]. We postulate that under 'high' CO_2 climate states prior to 24.5 Ma, only small regions of the AIS could advance into marine settings during cold astronomical configurations; warm seas precluded ice-sheet advance across the continental shelf. As CO_2 dropped below 600 ppm, ocean temperatures cooled and the AIS advanced across Antarctica's continental shelves, and connected increasingly larger areas of marine-based ice with the ocean. The maximum AIS extent during this phase of global cooling occurred between 23.2 and 23 Ma and is reflected by maxima in the $\delta^{18}O$ records[9,24,25]. The coincident increase in S_{obl} suggests that ocean-driven oscillations in the marine portions of the AIS were more strongly influenced by changes in the Earth's axial tilt.

Ice advanced into marine environments across the Ross Sea at 17.9 Ma (ref. [16]), as shown by a disconformity at 775 metres below the sea floor (mbsf) in the ANDRILL (AND)-2A drill core that coincides with Ross Sea seismic unconformity (RSU 4A). Deformed diamictite units overlie this disconformity and indicate that ice remained grounded near the drill site until 17.4 Ma. Subsequent ice-margin retreat to the coast is reflected by a change to more ice-distal glacimarine lithofacies in AND-2A (Figs. 1 and 3). An indirect record of the marine ice-sheet advance during this interval is captured in sediments and downhole geophysical data from Ocean Drilling Program (ODP) Site 1165[4] off Prydz Bay (Figs. 2 and 3). Most of the early-to-mid-Miocene record at this site comprises alternating facies of dark grey to black claystone with silt laminae and rare or absent ice-rafted debris (IRD) (Facies 1) and greenish grey bioturbated structureless claystone with common IRD (Facies 2). Peaks in downhole resistivity logs correlate with Facies 2 (ref. [4]). Resistivity data through the interval from ~750 to 500 mbsf includes a section of high variability (Fig. 3 and Supplementary Fig. 3) that records an increase in the Facies 2 unit thickness[4] and potentially reflects enhanced iceberg and sediment flux to the continental shelf margin due to more extensive and persistent ocean–ice sheet connections. These two records indicate that a marine ice-sheet advance occurred around Antarctica between ~18 and 17.4 Ma. These geological data coincide with an interval of high S_{obl} (Figs. 1 and 3) and offer additional evidence that S_{obl} is closely linked to the presence of extensive marine ice sheets on Antarctica's continental shelves. Far-field sea-level records preserved in stratigraphic sequences along the New Jersey margin[12] record a 10 to 15 m fall in relative sea level between 18 and 17.5 Ma, which supports the proximal geological evidence for an expanded AIS. This episode of sea-level fall follows a period of relatively stable sea level that coincides with low S_{obl} (Fig. 3). A 20 m rise in sea level approximately coincides with a decrease in S_{obl} that began at 17.4 Ma and is followed by another long interval of stable sea level that coincides with low S_{obl} (Fig. 3).

S_{obl} increased through the MCT, reaching maximum values at ~13.8 Ma, coincident with a large 1.5‰ shift in $\delta^{18}O$ (Fig. 1). Disconformities and proximal grounding-zone lithofacies dominate the Ross Sea drill core records through this interval[16,17] (Fig. 2) and erosional unconformities in seismic data indicate that marine ice sheets grounded across the continental shelf. Biological proxies suggest that sea ice became more temporally persistent across the MCT[16,26,27]. Atmospheric CO_2 concentrations dropped below 300 ppm between 14 and 13 Ma (ref. [28]). The MCT is interpreted to record another CO_2-controlled climatic threshold across which high-latitude surface temperatures decreased[29] and perennial sea ice grew around the Antarctic margin for the first time[16,27]. However, this climatic shift was transient as temperature increases in the late Miocene are reflected by a change from polar to subpolar glacial–marine lithofacies in the AND-1B drill core[17]. Despite this climatic rebound, geological records of late Miocene age are missing in drill core disconformities, which suggests that marine-based ice sheets became a more persistent feature after the MCT and repeatedly grounded across the shelf during the late Miocene. We infer that the increases in S_{obl} at ~9.5 Ma and ~5.8 Ma reflect episodes of decreased sea-ice extent. Although S_{obl} was variable through the late Miocene, it remained relatively low (compared to the early-to-mid-Miocene).

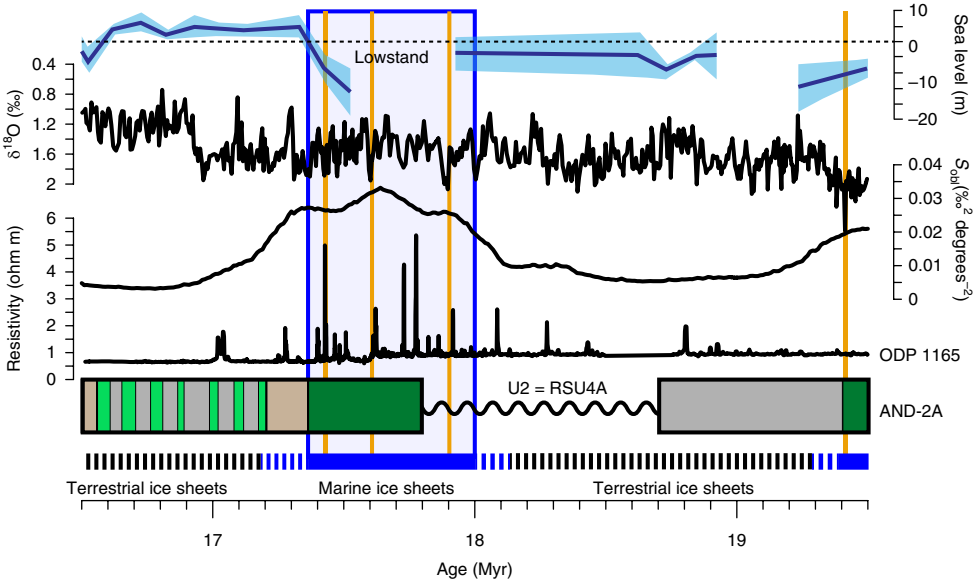

Fig. 3 | Correlation of Antarctic geological records and far-field data from the mid-Miocene. AND-2A drill core and downhole resistivity data from ODP Site 1165[4] correlated with S_{obl} and sea-level data from the New Jersey margin[12]. The colours in the drill core column represent the generalized stratigraphy (Fig. 1 caption). The vertical orange lines indicate inferred episodes of maximum marine ice-sheet advance, which coincide with peaks in S_{obl}, regional disconformities and $\delta^{18}O$ maxima. The blue box highlights an interval when the AIS extended across the continental shelf margins and marine ice sheets were a persistent feature. The blue envelope around the best-fit (blue line) sea-level curve captures the maximum and minimum estimates from Kominz et al.[12].

Ice-sheet response to increasing ocean connections

Our analysis indicates that the AIS was most sensitive to obliquity forcing when it advanced into marine environments, which suggest that ocean dynamics played a role in driving marine ice-sheet variability at a 41 kyr frequency. Studies of recent glacial dynamics[30,31] and ice-sheet modelling[32,33] indicate that ocean dynamics played a significant role in driving the marine-based ice-sheet retreat. However, analysis of ocean–ice interactions over long glacial–interglacial timescales using detailed physical models are not yet possible. We draw on modern observations and modelling studies of contemporary oceanographic processes across the Antarctic continental margin[34,35] to offer a conceptual model to explain how changes in obliquity could influence marine ice sheets (Fig. 4).

Obliquity affects Antarctica's marine ice sheets via its influence on the meridional temperature gradient. As the Earth's axial tilt increases, high latitudes warm, meridional temperature gradients decrease and zonal winds weaken[36]. Southward migration of the Southern Hemisphere westerly winds (SWW) increases wind stress above the Antarctic Circumpolar Current (ACC), which causes it to speed up[37]. Ekman transport north of the ACC increases, which enhances upwelling of the warm deep water in the southern limb of the overturning circulation[37]. At the same time, Antarctic easterlies weaken and migrate southwards, which causes isotherms along the Antarctic slope to shoal and thereby promote advection of warm water into grounding zones and ice-shelf cavities[34]. A decrease in wind shear stress across the Antarctic slope front causes shoaling of isopycnals and enhances the eddy-driven transport of warm water across the continental shelf margin[35]. During glacial intervals, these large-scale processes reverse as the Earth's tilt decreases and meridional temperature gradients increase. Northward migration and strengthening of zonal winds reduce the upwelling of warm water across the shelf. Periods of cold mean climate are characterized by extensive sea-ice growth, which further reduces the influence of zonal winds across the Antarctic slope and continental margin.

Our model identifies three phases of AIS evolution over the period 34–5 Ma (Fig. 4). Obliquity sensitivity during the early Oligocene was low because the circum-Antarctic Southern Ocean basin was still evolving, and Earth's climate state was too warm to support marine ice sheets (Fig. 4 (top)). Variation in the local insolation forcing due to 400 and 100 kyr eccentricity-modulated precession cycles and obliquity drove the terrestrial ice-sheet oscillations. By the late Oligocene, circum-Antarctic large-scale circulation patterns that characterize the modern Southern Ocean had been established[38]. Climatic cooling associated with a drop in atmospheric CO_2 allowed ice sheets to expand beyond their terrestrial margins and ground across areas of Antarctica's continental shelves. Glacial–interglacial advance and retreat of marine-based portions of the AIS were now influenced by obliquity-paced changes in ocean dynamics across the continental margin. This fundamental shift in AIS dynamics is reflected by an S_{obl} that became higher and more variable from 24 to 14 Ma (Figs. 1 and 4 (middle)). Water temperatures across the Ross Sea through this period varied between ~0 and 10 °C (ref. [16]) and suggest significant dynamic exchange between the Southern Ocean and Antarctic continental shelves. A general decrease in the long and short eccentricity variance in the $\delta^{18}O$ record, and an increase in the obliquity signal, occur after 13 Ma and persists through much of the late Miocene (Fig. 1). We posit that climatic cooling across the MCT decreased the influence of local insolation on surface melt and reduced the magnitude of terrestrial ice-sheet variability, which is reflected by a weakened 100 kyr eccentricity signal in the $\delta^{18}O$ record (Fig. 1a and Supplementary Fig. 4a). Oscillations in AIS volume and extent were now strongly influenced by changes in the marine-based ice in East and West Antarctica that were driven by obliquity-modulated upwelling of warm water from the circum-Antarctic Southern Ocean (Fig. 4 (bottom) and Supplementary Fig. 4c–e). Episodes of low S_{obl} in the late Miocene reflect times when the climate cooled and extensive sea ice developed to create a barrier that reduced the oceanic influence on ice-sheet variability (Fig. 4 (bottom)). During these cold episodes, marine ice-sheet variability and S_{obl} remained low. In contrast, during intervals when the climate warmed enough to melt sea ice but remained cold enough to maintain small marine ice sheets through

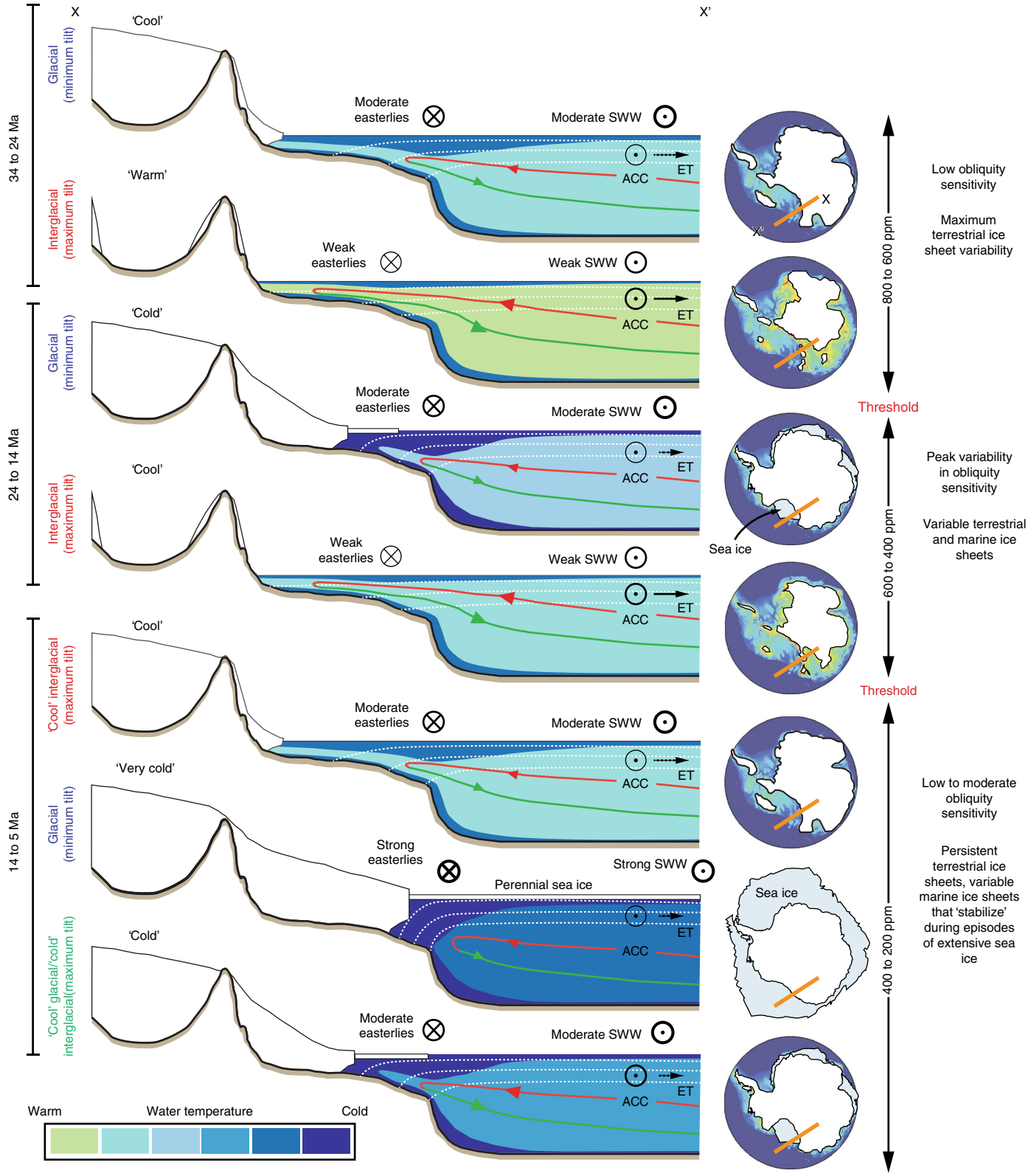

Fig. 4 | Conceptual model outlining the influence of obliquity on ice-sheet variability at glacial–interglacial frequencies as the AIS evolved over the past 34 million years under high, medium and low atmospheric CO_2 conditions. The positions of the cross-sections X–X′ are indicated by orange lines on the maps. The general position of the zonal wind systems is indicated by circles with crosses (easterlies heading into the page) and dots (westerlies heading out of page); the strength is indicated by line thickness (the heavier, the stronger). ET, Ekman transport (dashed arrows show a weaker flow). ACC, Antarctic Circumpolar Current. SWW, south westerly winds. Red and green lines represent the overturning circulation (larger arrows show an enhanced upwelling). Dark blue 'lenses' represent cold, dense bottom water and low salinity surface water. Generic isotherms are shown by dashed white lines.

interglacial intervals (e.g. ~10 to 8 Ma), marine ice sheets remained connected to obliquity-driven changes in ocean dynamics, and variations in S_{obl} reflect changes in obliquity-forcing variance.

If sea-ice cover decreases in the coming decades, our results suggest that the enhanced oceanic-heat delivery (modulated by present-day obliquity forcing) will facilitate ocean-driven melt at the AIS margin. Antarctica's continental shelves now deepen inland, which creates a dynamical instability that enhances the marine ice-sheet retreat and volume loss. Our data support recent ice-sheet model simulations[33,39] and imply that the stabilization or reduction of atmospheric CO_2 is required to avoid the loss of ice shelves and the retreat of Antarctica's marine ice sheets.

Online content

Any methods, additional references, Nature Research reporting summaries, source data, statements of data availability and associated accession codes are available at https://doi.org/10.1038/s41561-018-0284-4.

Received: 2 May 2018; Accepted: 26 November 2018;
Published online: 14 January 2019

References

1. DeConto, R. M. & Pollard, D. Rapid Cenozoic glaciation of Antarctica induced by declining atmospheric CO_2. *Nature* **421**, 245–249 (2003).
2. Zhang, Y. G., Pagani, M., Liu, Z., Bohaty, S. M. & DeConto, R. A 40-million-year history of atmospheric CO_2. *Phil. Trans. R. Soc.* **371**, 20130096 (2013).
3. Lawver, L. A. & Gahagan, L. M. Evolution of Cenozoic seaways in the circum-Antarctic region. *Palaeogeogr. Palaeoclimatol. Palaeoecol.* **198**, 11–37 (2003).
4. Williams, T. & Handwerger, D. A high-resolution record of early Miocene Antarctic glacial history from ODP Site 1165, Prydz Bay. *Paleoceanography* **20**, PA2017 (2005).
5. Galeotti, S. et al. Antarctic ice sheet variability across the Eocene–Oligocene boundary climate transition. *Science* **352**, 76–80 (2016).
6. Naish, T. et al. Obliquity-paced Pliocene West Antarctic Ice Sheet oscillations. *Nature* **458**, 322–328 (2009).
7. De Vleeschouwer, D., Vahlenkamp, M., Crucifix, M. & Pälike, H. Alternating Southern and Northern Hemisphere climate response to astronomical forcing during the past 35 m.y. *Geology* **45**, 375–378 (2017).
8. Pälike, H. et al. The heartbeat of the Oligocene climate system. *Science* **314**, 1894–1898 (2006).
9. Liebrand, D. et al. Cyclostratigraphy and eccentricity tuning of the early Oligocene through early Miocene (30.1–17.1 Ma): Cibicides mundulus stable oxygen and carbon isotope records from Walvis Ridge Site 1264. *Earth Planet. Sci. Lett.* **450**, 392–405 (2016).
10. Holbourn, A., Kuhnt, W., Clemens, S., Prell, W. & Andersen, N. Middle to late Miocene stepwise climate cooling: evidence from a high-resolution deep water isotope curve spanning 8 million years. *Paleoceanography* **28**, 688–699 (2013).
11. Laskar, J., Robutel, P., Gastineau, M., Correia, A. C. M. & Levrard, B. A long term numerical solution for the insolation quantities of the Earth. *Astron. Astrophys.* **428**, 261–285 (2004).
12. Kominz, M. A., Miller, K. G., Browning, J. V., Katz, M. E. & Mountain, G. S. Miocene relative sea level on the New Jersey shallow continental shelf and coastal plain derived from one-dimensional backstripping: a case for both eustasy and epeirogeny. *Geosphere* **12**, 1437–1456 (2016).
13. De Santis, L., Prato, S., Brancolini, G., Lovo, M. & Torelli, L. The eastern Ross Sea continental shelf during the Cenozoic: implications for the West Antarctic Ice Sheet development. *Glob. Planet. Change* **23**, 173–196 (1999).
14. Sorlien, C. C. et al. Oligocene development of the West Antarctic Ice Sheet recorded in eastern Ross Sea strata. *Geology* **35**, 467–470 (2007).
15. Bart, P. J. & De Santis, L. Glacial intensification during the Neogene: a review of seismic stratigraphic evidence from the Ross Sea, Antarctica, continental shelf. *Oceanography* **25**, 166–183 (2012).
16. Levy, R. et al. Antarctic ice sheet sensitivity to atmospheric CO_2 variations in the early to mid-Miocene. *Proc. Natl Acad. Sci. USA* **113**, 3453–3458 (2016).
17. McKay, R. et al. The stratigraphic signature of the late Cenozoic Antarctic ice sheets in the Ross Embayment. *Geol. Soc. Am. Bull.* **121**, 1537–1561 (2009).
18. Anderson, J. B. et al. Progressive Cenozoic cooling and the demise of Antarctica's last refugium. *Proc. Natl Acad. Sci. USA* **108**, 11356–11360 (2011).
19. Hambrey, M. J. et al. Cenozoic glacial record of the Prydz Bay continental shelf, East Antarctica. *Proc. Ocean Drilling Program, Scientific Results* **119**, 77–132 (1991).
20. Florindo, F. et al. Magnetobiostratigraphic chronology and palaeoenvironmental history of Cenozoic sequences from ODP sites 1165 and 1166, Prydz Bay, Antarctica. *Palaeogeogr. Palaeoclimatol. Palaeoecol.* **198**, 69–100 (2003).
21. Scher, H. D., Bohaty, S. M., Zachos, J. C. & Delaney, M. L. Two-stepping into the icehouse: East Antarctic weathering during progressive ice-sheet expansion at the Eocene–Oligocene transition. *Geology* **39**, 383–386 (2011).
22. Barrett, P. J. Textural characteristics of Cenozoic preglacial and glacial sediments at Site 270, Ross Sea, Antarctica. *Initial Rep. Deep Sea Drilling Project* **28**, 757–766 (1975).
23. Naish, T. R., Wilson, G. S., Dunbar, G. B. & Barrett, P. J. Constraining the amplitude of Late Oligocene bathymetric changes in western Ross Sea during orbitally-induced oscillations in the East Antarctic Ice Sheet: (2) implications for global sea-level changes. *Palaeogeogr. Palaeoclimatol. Palaeoecol.* **260**, 66–76 (2008).
24. Zachos, J. C., Shackleton, N. J., Revenaugh, J. S., Pälike, H. & Flower, B. P. Climate response to orbital forcing across the Oligocene–Miocene boundary. *Science* **292**, 274–278 (2001).
25. Beddow, H. M., Liebrand, D., Sluijs, A., Wade, B. S. & Lourens, L. J. Global change across the Oligocene–Miocene transition: high-resolution stable isotope records from IODP Site U1334 (equatorial Pacific Ocean). *Paleoceanography* **31**, 81–97 (2016).
26. Crampton, J. S. et al. Southern Ocean phytoplankton turnover in response to stepwise Antarctic cooling over the past 15 million years. *Proc. Natl Acad. Sci. USA* **113**, 6868–6873 (2016).
27. Sangiorgi, F. et al. Southern Ocean warming and Wilkes Land ice sheet retreat during the mid-Miocene. *Nat. Commun.* **9**, 317 (2018).
28. Badger, M. P. S. et al. CO_2 drawdown following the middle Miocene expansion of the Antarctic Ice Sheet. *Paleoceanography* **28**, 42–53 (2013).
29. Lewis, A. R. et al. Mid-Miocene cooling and the extinction of tundra in continental Antarctica. *Proc. Natl Acad. Sci. USA* **105**, 10676–10680 (2008).
30. Shepherd, A., Wingham, D. & Rignot, E. Warm ocean is eroding West Antarctic Ice Sheet. *Geophys. Res. Lett.* **31**, L23402 (2004).
31. Hillenbrand, C.-D. et al. West Antarctic Ice Sheet retreat driven by Holocene warm water incursions. *Nature* **547**, 43–48 (2017).
32. Golledge, N. R., Levy, R. H., McKay, R. M. & Naish, T. R. East Antarctic ice sheet most vulnerable to Weddell Sea warming. *Geophys. Res. Lett.* **44**, 2343–2351 (2017).
33. DeConto, R. M. & Pollard, D. Contribution of Antarctica to past and future sea-level rise. *Nature* **531**, 591–597 (2016).
34. Spence, P. et al. Rapid subsurface warming and circulation changes of Antarctic coastal waters by poleward shifting winds. *Geophys. Res. Lett.* **41**, 4601–4610 (2014).
35. Stewart, A. L. & Thompson, A. F. Eddy-mediated transport of warm Circumpolar Deep Water across the Antarctic Shelf Break. *Geophys. Res. Lett.* **42**, 432–440 (2014).
36. Timmermann, A. et al. Modeling obliquity and CO_2 effects on Southern Hemisphere climate during the past 408 ka. *J. Clim.* **27**, 1863–1875 (2014).
37. Toggweiler, J. R. & Russell, J. Ocean circulation in a warming climate. *Nature* **451**, 286–288 (2008).
38. Pfuhl, H. A. & McCave, I. N. Evidence for late Oligocene establishment of the Antarctic Circumpolar Current. *Earth. Planet. Sci. Lett.* **235**, 715–728 (2005).
39. Golledge, N. R. et al. The multi-millennial Antarctic commitment to future sea-level rise. *Nature* **526**, 421–425 (2015).

Acknowledgements

This study was supported by the New Zealand Ministry of Business Innovation and Employment contract C05X1001 (R.H.L., T.R.N., N.R.G. and R.M.M.) and by NSF grant EAR-1151438 (S.R.M.). A sabbatical leave from the University of Wisconsin—Madison supported S.R.M to conduct research at the Institute of Geological and Nuclear Science.

Author contributions

R.H.L. and S.R.M. conceived the project. R.H.L., T.R.N. and R.M.M. performed the stratigraphic and proxy synthesis, and S.R.M. conducted the time series analyses. R.H.L. and S.R.M. wrote the first draft of the manuscript, in consultation with T.R.N., N.R.G., J.S.C. and R.M.M. All the authors contributed to the interpretations and major findings of this work.

Competing interests

The authors declare no competing interests.

Additional information

Supplementary information is available for this paper at https://doi.org/10.1038/s41561-018-0284-4.

Reprints and permissions information is available at www.nature.com/reprints.

Correspondence and requests for materials should be addressed to R.H.L.

Publisher's note: Springer Nature remains neutral with regard to jurisdictional claims in published maps and institutional affiliations.

Methods

Obliquity sensitivity. We define $\delta^{18}O$ obliquity sensitivity (S_{obl}) as:

$$S_{obl} = \frac{\sigma^2_{\delta^{18}O}}{\sigma^2_{La04}}$$

where $\sigma^2_{\delta^{18}O}$ is the obliquity variance in the $\delta^{18}O$ megasplice[7], in units of ‰^{2}, and σ^2_{La04} is the variance of the theoretical obliquity solution[11], in units of degrees^2. The multitaper method time–frequency power spectrum integration was utilized to quantify S_{obl} (refs. [40,41]). To isolate the dominant 41 kyr obliquity signal, the spectrum integration was conducted from 0.023 to 0.027 cycles kyr^{-1} (~43.5 to 37 kyr). All the time–frequency analyses employed three 2π prolate data tapers, with a 1 Myr window and a 10 kyr time step; a linear trend was removed from each 1 Myr window prior to analysis.

The $\delta^{18}O$ megasplice is characterized by variable sampling resolution, with a median resolution of 2.38 kyr. Larger sample spacing through portions of the record could diminish the obliquity signal strength. To compensate for this, the theoretical obliquity solution[11] was resampled on the temporal grid of the $\delta^{18}O$ megasplice. Both the megasplice and resampled obliquity solution were then interpolated using a 2.5 kyr grid (Supplementary Fig. 4c, black line). A reduction in the $\delta^{18}O$ obliquity strength ($\sigma^2_{\delta^{18}O}$) due to a coarser resolution sampling is compensated by a reduction in σ^2_{La04}.

To further evaluate the impact of the megasplice sampling grid on our conclusions, we conducted two additional sensitivity analyses: (1) we evaluated the fraction of the 40 kyr variance that is recovered from the resampled theoretical obliquity solution after the application of the megasplice temporal grid, and (2) we compared S_{obl} analyses using both the resampled and unresampled obliquity solution (Supplementary Fig. 4c). These analyses confirm that our assessment of $\sigma^2_{\delta^{18}O}$ and S_{obl} is robust for portions of the record younger than 33.87 Ma, where >70% of the 40 kyr variance is recovered in each 1 Myr window (with an average of 91 ± 6% for the entire interval from 2.59 to 33.87 Ma (1σ)).

To compliment this assessment of S_{obl}, we evaluated the magnitude of the $\delta^{18}O$ obliquity variance relative to the $\delta^{18}O$ precession variance (Supplementary Fig. 4d), and also relative to the combined $\delta^{18}O$ precession +$\delta^{18}O$ eccentricity variance (Supplementary Fig. 4e). Precession variance is quantified via a power spectrum integration from 0.04 to 0.06 cycles kyr^{-1} (~25 to 17 kyr), and eccentricity variance is determined via integration from 0 to 0.012 cycles kyr^{-1} (the length of the window, 1 Myr, to ~83 kyr).

We recognize that the number of high-resolution astronomically tuned data sets suitable for a reliable S_{obl} assessment is small, given the required temporal resolution. Even in cases where sampling resolution is high, low sedimentation rates combined with bioturbation can obscure the true magnitude of obliquity forcing. The megasplice[7] was constructed from nine records with an objective of maximizing the time resolution and we consider it the best-available estimate of S_{obl}. However, to examine the impact of regional influences and megasplice stitching points on the observed S_{obl} we provide complimentary analyses of new data sets from ODP Sites 982 (North Atlantic)[42], 1146 (South China Sea)[43], 1264 (South Atlantic Walvis Ridge)[9] and legacy data from 1218 (equatorial Pacific)[8]. The new data set from Site 982 is an update of prior work (used in the megasplice), which includes splice revisions, new oxygen isotope data and a new astronomical tuning;[39] these results are consistent with the megasplice (Supplementary Fig. 5). The new data set from Site 1146[40] allows a comparison with the uppermost Miocene Site 982 data (<8.56 Ma) used in the megasplice, and Site U1338 data (>12.825 Ma (equatorial Pacific))[44] used in the original megasplice. The results from Site 1146 confirm the presence of an enhanced S_{obl} at 5.9, 9.2 and 14 Ma (Supplementary Fig. 5d), in addition to the increases in S_{obl} at 7.7 and 15.9 Ma. Importantly, the largest S_{obl} occurs prior to 13 Ma, consistent with our interpretation of marine-based ice sheets with minimal sea-ice fields.

The new data set[9] from South Atlantic Site 1264/1265 is characterized by extremely low sedimentation rates (<1 cm kyr^{-1}), and thus should be approached with caution. As expected, we observed an overall reduced magnitude of S_{obl}, consistent with low sedimentation rates and bioturbation that obscure the high-frequency obliquity forcing (Supplementary Fig. 5e). Nonetheless, the overall features observed in the Site 1264/1265 S_{obl} are generally consistent with the megasplice. The most substantial mismatch is within the interval from 22 to 24.5 Ma, in which the megasplice shows a strong increase in S_{obl}, whereas Site 1264/1265 has a delayed maximum. Note, however, that the highest values of S_{obl} occur within the Miocene, consistent with our evaluation of the megasplice.

Finally, a complementary analysis of Site 1218 is included, using the original manually tuned astrochronology of Pälike et al.[8]. This permits the analysis of a single record across the Oligocene–Miocene boundary. The results reveal a good agreement with the megasplice, and an increase in S_{obl} at the Oligocene–Miocene boundary, although the obliquity response is probably muted by low sedimentation rates and reduced data resolution (Supplementary Fig. 5f).

Based on these new analyses, we conclude that there is robust evidence for the major S_{obl} features discussed in this work. As illustrated in Figs. 1 and 4, the evaluation of S_{obl} provides a 1 Myr average of different AIS ice-extent scenarios, and thus integrates a wide range of spatial variability on shorter time scales; these averages potentially include outliers in some sectors of Antarctica, which we cannot discern at present. The assessment of S_{obl} in future studies and the integration with high-resolution studies of proximal geological records will permit further constraint and evaluation of the model for AIS development proposed here.

All analyses utilize the Astrochron software for R[45,46]; a script is included in the Supplementary Information.

Ross Sea stratigraphy. The correlations presented in Fig. 1 primarily utilize published data[5,16,23]. However, recent biostratigraphic analysis of DSDP 270 identified key biostratigraphic data that identify a major disconformity (270-U2) at ~112 mbsf and constrain its duration from ~23 to 21 Ma (Supplementary Table 1). The ages for key diatom data reported in DSDP 272[47] are updated based on recent revisions to the Southern Ocean diatom biostratigraphy and chronostratigraphy[26,48]. All the key events and horizons, their ages and the relevant references are presented in Supplementary Table 1.

ODP Site 1165. A revised age model for ODP Site 1165 is established herein (Supplementary Fig. 3 and Supplementary Table 2). Whereas the model uses previously published magnetostratigraphy and diatom occurrences[20], the maximum and minimum age range reported for the diatom data are derived from the total, average and hybrid range models of Florindo et al.[48]. We used the hybrid range model ages for tie points (marked by the base of the arrows in Supplementary Fig. 3) to guide the correlation of the magnetic polarity reversals to the global polarity timescale[49]. Key tie points from this revised age model were used to correlate downhole resistivity data from Site 1165[4] to the AND-2A drill core and the S_{obl} curve (Fig. 3).

Diatom turnover. The diatom origination plus extinction (turnover) rate (Fig. 1 and Supplementary Fig. 2) was constructed from diatom occurrences recorded in drill cores from the Antarctic margin and Southern Ocean and is expressed as the lineage million-year rate that is insensitive to the overall diversity[50]. The turnover curve plotted is the ensemble median derived by bootstrap resampling of three models of diatom first and last occurrences in the Southern Ocean. The three models are based on 27 or 34 drill cores. This model ensemble approach captures uncertainties related to the position of the polar front over time, the nature of biases that affect the fossil record, the age calibration of drill cores and the selection of species used in the analysis. Methodology and time series from 0 to 15 Ma are published[26], but the data series is extended here to 26 Ma and includes a major turnover event between 23.9 and 23.65 Ma (Fig. 1 and Supplementary Fig. 2). Major turnover events coincide with proxy evidence for cooling and were driven by expansion of Antarctica's marine-based ice sheets and sea ice[26].

Data availability

Data sets generated during and/or analysed during the current study are available in Supplementary Tables 1 and 2 or from the corresponding author on reasonable request.

References

40. Thomson, D. J. Spectrum estimation and harmonic analysis. *Proc. IEEE* **70**, 1055–1096 (1982).
41. Meyers, S. R., Sageman, B. B. & Arthur, M. A. Obliquity forcing of organic matter accumulation during Oceanic Anoxic Event 2. *Paleoceanography* **27**, PA3212 (2012).
42. Drury, A. J. et al. Deciphering the state of the late Miocene to early Pliocene equatorial Pacific. *Paleoceanogr. Paleoclimatol.* **33**, 246–263 (2018).
43. Holbourn, A. E. et al. Late Miocene climate cooling and intensification of southeast Asian winter monsoon. *Nat. Commun.* **9**, 1584 (2018).
44. Holbourn, A. et al. Middle Miocene climate cooling linked to intensification of eastern equatorial Pacific upwelling. *Geology* **42**, 19–22 (2014).
45. *R: A Language and Environment for Statistical Computing* (R Foundation for Statistical Computing, 2016).
46. Meyers, S. R. *Astrochron: an R package for Astrochronology* (R Project for Statistical Computing, 2014).
47. Savage, M. L. & Ciesielski, P. F. in *Antarctic Earth Science* (eds Oliver, R. L., James, P. R. & Jago, J. B.) 555–559 (Australian Academy of Science, Canberra, 1983).
48. Florindo, F. et al. Paleomagnetism and biostratigraphy of sediments from Southern Ocean ODP Site 744 (southern Kerguelen Plateau): implications for early-to-middle Miocene climate in Antarctica. *Glob. Planet. Change* **110**, 434–454 (2013).
49. Gradstein, F. M. et al. in *The Geologic Time Scale* (eds Gradstein, F. M., Ogg, J. G, Schmitz, D. & Ogg, M.) ix–xi (Elsevier, Amsterdam, 2012).
50. Raup, D. M. Mathematical models of cladogenesis. *Paleobiology* **11**, 42–52 (1985).